

Efficiency Enhancement of Organic Solar Cells by Using Shape-Dependent Broadband Plasmonic Absorption in Metallic Nanoparticles

Xuanhua Li, Wallace Chik Ho Choy,* Haifei Lu, Wei E. I. Sha, and Aaron Ho Pui Ho

It is been widely reported that plasmonic effects in metallic nanomaterials can enhance light trapping in organic solar cells (OSCs). However, typical nanoparticles (NP) of high quality (i.e., mono-dispersive) only possess a single resonant absorption peak, which inevitably limits the power conversion efficiency (PCE) enhancement to a narrow spectral range. Broadband plasmonic absorption is obviously highly desirable. In this paper, a combination of Ag nanomaterials of different shapes, including nanoparticles and nanoprisms, is proposed for this purpose. The nanomaterials are synthesized using a simple wet chemical method. Theoretical and experimental studies show that the origin of the observed PCE enhancement is the simultaneous excitation of many plasmonic low- and high-order resonances modes, which are material-, shape-, size-, and polarization-dependent. Particularly for the Ag nanoprisms studied here, the high-order resonances result in higher contribution than low-order resonances to the absorption enhancement of OSCs through an improved overlap with the active material absorption spectrum. With the incorporation of the mixed nanomaterials into the active layer, a wide-band absorption improvement is demonstrated and the short-circuit photocurrent density (J_{sc}) improves by 17.91%. Finally, PCE is enhanced by 19.44% as compared to pre-optimized control OSCs. These results suggest a new approach to achieve higher overall enhancement through improving broadband absorption.

1. Introduction

Light trapping is an important topic for thin-film organic solar cells (OSCs) to improve light absorption and thus performance.^[1–3] Recently, metallic nanomaterial-enabled localized plasmonic resonances (LPRs) have been used to improve light trapping in OSCs.^[2–19] Especially, from a material point of view, silver (Ag) shows a most effective optical trapping

potential due to its relative stronger scattering efficiency among noble metals in the visible range.^[20–24] Some reports of metallic nanoparticle organic solar cells have adopted physical methods, such as thermal evaporation or electrodeposition, to form the metallic nanoparticles.^[25–27] Concerning solution-processed metallic nanoparticles, such as gold or silver nanoparticles, they are attractive candidates for study as optical antennae and scattering centers in organic photovoltaics because they can be processed from a variety of aqueous and organic solutions and can be synthesized in a variety of dimensions and geometries for achieving different optical properties.^[9–13,28–33] By appropriately designing metallic nanomaterial geometries, researchers would like to enhance the scattering of incident light into the intrinsic absorbing layer, increasing the optical path length and improving the light absorption within the absorbing layer. However, the resonant wavelength region of metallic nanomaterials is typically narrow, being determined by the nanomaterials size and shape, and the local dielectric environment,^[5,34]

which inevitably limits the power conversion efficiency (PCE) enhancement to a narrow spectral range. Meanwhile, sunlight is a broadband light source. It is desirable to extend the wavelength region of enhanced light absorption by using plasmonic nanostructures.^[2,35,36]

To achieve a broadband absorption enhancement in OSCs, the plasmonic nanostructures need to be able to strongly scatter the incident solar light into a large wavelength range so that light can be best trapped inside the active layer. Previous attempts mainly focused on regularly patterned gratings with rigorous geometrical precision requirements.^[2,8,11] Although this approach promises both theoretically and experimentally to achieve considerable efficiency enhancements, these attempts involve sophisticated and expensive lithography fabrication. In comparison, the self-assembly and wet chemical synthesis methods present a simple and less expensive option.^[20]

In this paper, we propose and demonstrate a new method based on combining differently shaped nanomaterials of Ag nanoparticles and Ag nanoprisms to achieve broad spectral enhancement range. These nanomaterials are realized by

X. H. Li, Prof. W. C. H. Choy, Dr. W. E. I. Sha
Department of Electrical and Electronic Engineering
the University of Hong Kong
Pokfulam Road, Hong Kong, P. R. China
E-mail: chchoy@eee.hku.hk

H. F. Lu, Prof. A. H. P. Ho
Department of Electronic Engineering
Center for Advanced Research in Photonics
the Chinese University of Hong Kong
Shatin, NT, Hong Kong SAR, 852, P. R. China



DOI: 10.1002/adfm.201202476

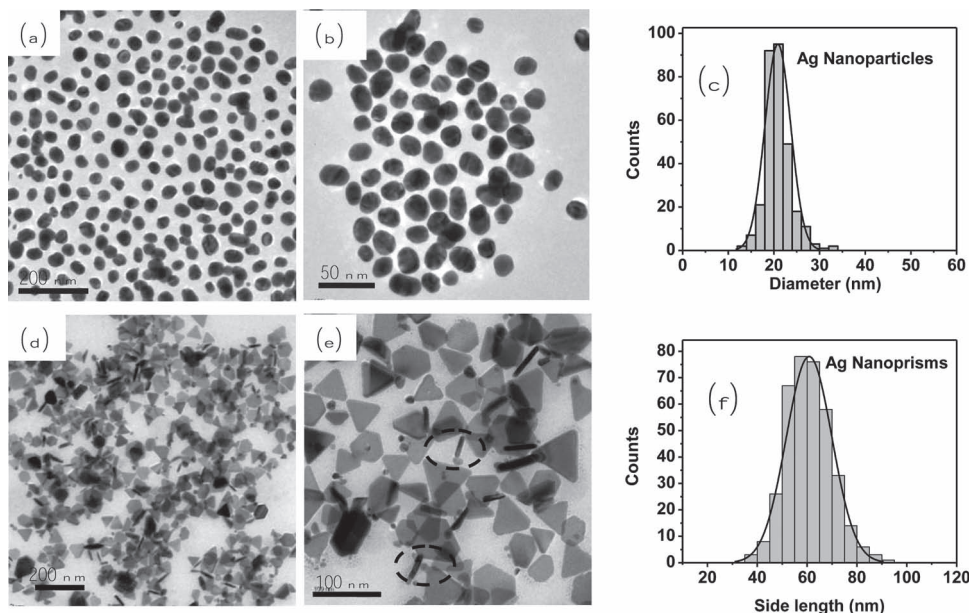


Figure 1. TEM micrographs of the shape-controllable Ag nanomaterials synthesized by wet-chemistry method: a,b) spherical Ag nanoparticles; and, d, e) triangular Ag nanoprisms. c,f) Size-distribution histogram of the as-prepared Ag nanoparticles and Ag nanoprisms, respectively. In (e), it should be noted that the 'rod'-shaped Ag nanomaterials in the TEM marked by black circles are not nanorods but are vertically oriented nanoprisms.

the simple and low-cost wet chemical synthesis methods and can be readily scaled up for full-size solar cell fabrication. We theoretically and experimentally study the incorporation of the mixed nanomaterials with broadband optical response into the active layer and show broadband absorption enhancement, as well as the origin of this enhancement. Our results demonstrate a short-circuit photocurrent density (J_{sc}) enhancement of 17.91% and a power conversion efficiency (PCE) enhancement of 19.44%, as compared to pre-optimized control OSCs.

2. Results and Discussion

Figure 1 shows the transmission electron microscopy (TEM) images and size distribution of synthesized Ag nanoparticles and Ag nanoprisms. By counting about 300 Ag nanoparticles and Ag nanoprisms from TEM images of each sample, we statistically obtain the size distribution of the products as shown in **Figure 1c** and **f**. According to the transmission electron microscopy (TEM) images and size distribution, the diameter of Ag nanoparticles is about 20 nm and the side length and thickness of Ag nanoprisms are around 60 and 10 nm, respectively. To analyze the LPR characteristics, the absorption spectra of synthesized Ag nanomaterials dispersed in water were measured, as shown in **Figure 2a**. Ag nanoparticles and nanoprisms have maximum absorption peaks around 400 and 600 nm, respectively, which arise from the LPRs of two different shapes of NPs. After mixing the

two shaped Ag NPs, a broader absorption spectrum is obtained, covering the range 400 to 600 nm. By using the combined Ag nanomaterials in the active layer of OSCs, we would like to achieve a broad wavelength range of absorption enhancement. **Figure 3a** and **b** show scanning electron microscopy (SEM) top-view and cross-sectional images of the active layer incorporating mixed Ag nanomaterials with 2 wt% Ag nanoparticles and 2 wt% Ag nanoprisms. The small Ag nanoparticles, of about 20 nm, and large Ag nanoprisms, about 60 nm side length, are well observed in the active layer. These images confirm that the Ag nanoparticles and nanoprisms can be well dispersed yet retain their particular shape and size within the active layer. Furthermore, in order to study the film quality of P3HT:PCBM with or without Ag nanomaterials, we provide atomic force microscopy (AFM) images of the pristine film and the film with Ag nanomaterials. According to the AFM images shown in **Figure 3c,d**, the root-mean-square (rms) roughness

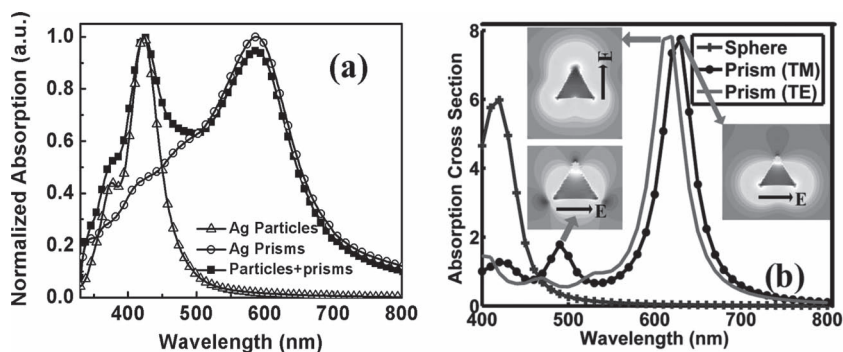


Figure 2. a) Experimental and b) theoretical absorption of Ag nanoparticles and Ag nanoprisms in water. The insets of (b) are E -field distributions at the resonance peaks of 500 and 630 nm with the same polarization direction.

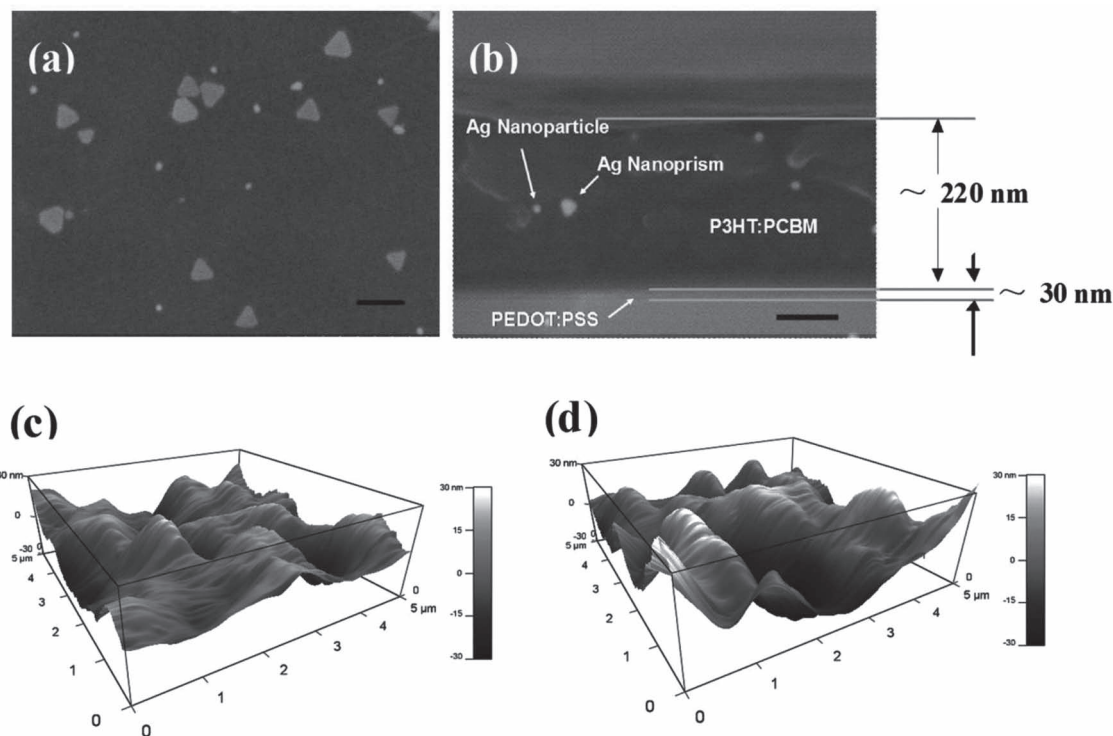


Figure 3. a) Top-view, and, b) cross-sectional SEM images of P3HT:PCBM film incorporated with mixed Ag nanoparticles and nanoprisms. The scale bar is 100 nm. 3D AFM images of: c) pristine P3HT:PCBM film, and, d) P3HT:PCBM film with Ag nanomaterials (2 wt%).

of the film slightly increases from 11.707 nm (pristine) to 14.257 nm (with Ag nanomaterials); thus, the Ag nanomaterials incorporated into the active layer should not significantly modify the film.

To elucidate the absorption spectra of the Ag nanoparticles and nanoprisms, a 3D volume integral equation method is used to theoretically model their optical response, as shown in Figure 2b. The theoretical spectra confirm and explain the experimental results. From theoretical studies, we show that a nanoprism has polarization-dependent LPR around 620 nm when incident light is polarized along different main axes of the triangle surface. Interestingly, one can observe a lot of small resonance peaks associated with the nanoprism before 600 nm, which are attributed to high-order plasmonic resonances. Compared with the dipole (low-order) plasmonic resonance, the high-order plasmonic resonances have more complex scattering pattern with different angular momentum (see *E*-field distributions at the resonance peaks of 500 and 630 nm with the same polarization direction as shown in Figure 2b).

The basic OSC structure is ITO/PEDOT:PSS (30 nm)/P3HT:PCBM (220 nm):Ag nanomaterials/Ca (80 nm)/Al (100 nm). The Ag nanomaterials include Ag nanoparticle only, Ag nanoprisms only, or mixed Ag nanoparticles and Ag nanoprisms. In order to optimize OSC performances via achieving broadband absorption based on the optical effect of Ag nanomaterials, we first optimize OSC performance with one type of Ag nanomaterial (i.e., Ag nanoparticles only or Ag nanoprisms only). Then, we investigate the effects of the mixed Ag structures (i.e., both

Ag nanoparticles and Ag nanoprisms) on OSC performances. The corresponding current density–voltage (*J*–*V*) characteristics of the optimized devices with or without Ag nanomaterials are shown in Figure 4, with their performance summarized in Table 1. The optimized reference device shows a PCE of 3.6%. For the optimized (2 wt%) Ag nanoparticle-only and optimized (2 wt%) Ag nanoprism-only cases, the OSCs have improved PCEs of 3.99% and 4.07%, respectively. Furthermore, for the optimized mixed Ag nanomaterial (2 wt% Ag nanoparticle and 2 wt% Ag nanoprisms) case, the optimized PCE reaches 4.3%.

Optimization details of device performance with various concentrations of Ag nanoparticles only, Ag nanoprisms only, and the mixed case are shown in Tables S1 to S3 and Figures S1 to S3 in the Supporting Information. The results show that the concentration of Ag nanomaterials incorporated into the active layer will obviously affect the OSC performance. At low concentration of Ag nanomaterials, the absorption of OSCs will have less enhancement, and a relatively small J_{sc} improvement (e.g., for 1 wt% Ag nanoparticles, J_{sc} and PCE increase to 9.32 mA cm⁻² and 3.86%, respectively, from 8.99 mA cm⁻² and 3.6% in the control device). At high concentration, the absorption of OSCs continuously increases to higher value. However, OSCs will have degraded electrical properties, and encounter deterioration of device performances (e.g., for 5 wt% Ag nanoparticles, J_{sc} and PCE drastically decrease to 3.83 mA cm⁻² and 1.19%, respectively). At optimized concentration, improvement can be obtained in both the J_{sc} and FF, while the V_{oc} remains similar to that of the control device (e.g., Ag nanoparticles with

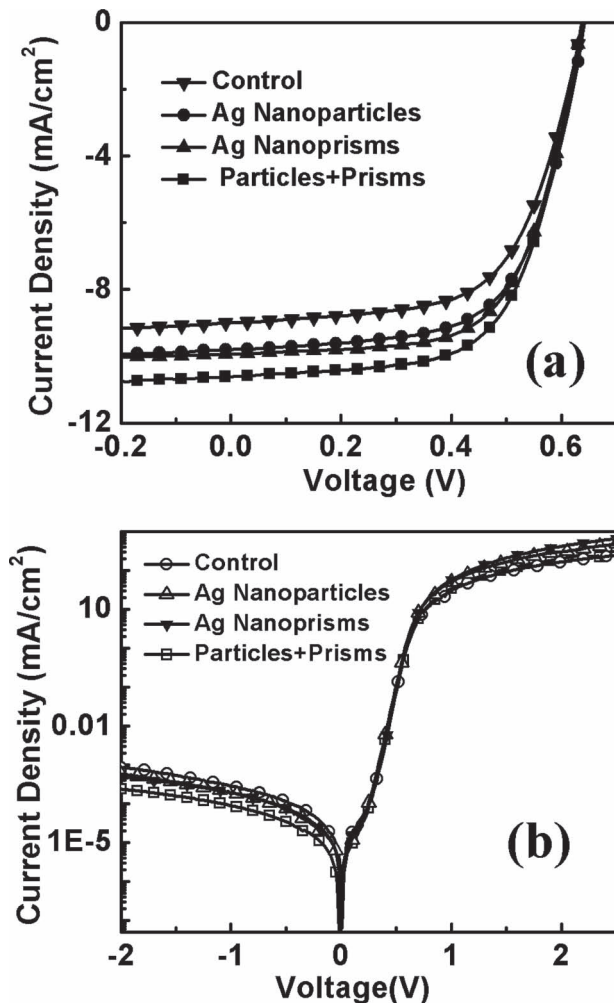


Figure 4. Current density–voltage (J – V) characteristics of devices with or without Ag nanomaterial incorporated into the active layers measured: a) under AM 1.5 illumination at 100 mW cm^{-2} , and, b) without illumination.

optimized concentration of 2 wt%, J_{sc} and FF clearly increase to 9.80 mA cm^{-2} and 0.636, respectively, from 8.99 mA cm^{-2} and 0.623 in the control device). The optimized J_{sc} values of OSCs with Ag nanoparticles only, Ag nanoprisms only, and the mixed Ag structures are 9.80, 9.93, and 10.61 mA cm^{-2} with

ca. 9.0%, 10.1%, and 17.91% enhancement, respectively, compared to the control device. The higher FF can be explained by the increased charge transport and induced R_s .^[2,3,7,23,37] In the current work, the improved charge transport can be shown from the improved hole mobility from $1.14 \times 10^{-7} \text{ m}^2 \text{ V}^{-1} \text{ s}^{-1}$ (control) to $2.23 \times 10^{-7} \text{ m}^2 \text{ V}^{-1} \text{ s}^{-1}$ (Ag nanoparticles), $2.59 \times 10^{-7} \text{ m}^2 \text{ V}^{-1} \text{ s}^{-1}$ (Ag nanoprisms), and $1.66 \times 10^{-7} \text{ m}^2 \text{ V}^{-1} \text{ s}^{-1}$ (mixed Ag nanoparticles and Ag nanoprisms), determined by the space-charge-limited current (SCLC) model together with hole-dominated devices with structures of ITO/PEDOT:PSS (30 nm)/P3HT:PCBM (220 nm) with and without Ag nanomaterials/MoO₃(15 nm)/Ag.^[38] Similarly, the electron mobility increase from $2.41 \times 10^{-7} \text{ m}^2 \text{ V}^{-1} \text{ s}^{-1}$ to 3.21×10^{-7} , 3.47×10^{-7} and $2.80 \times 10^{-7} \text{ m}^2 \text{ V}^{-1} \text{ s}^{-1}$ determined from electron-dominated devices with structures of ITO/TiO₂/P3HT:PCBM with and without Ag nanoparticles, Ag nanoprisms, or mixed Ag nanoparticles and Ag nanoprisms/Ca/Al. The Ag nanomaterials are 2 wt% Ag nanoparticles only, 2 wt% Ag nanoprisms only, and mixed 2 wt% Ag nanoparticles and 2 wt% Ag nanoprisms. As a result, the increased carrier transport and better balance of hole and electron mobilities contribute to the enhanced FF. More details of the results are described in Figure S4 in the Supporting Information.

To understand the optical effects of Ag nanomaterials, we study the absorption spectra of P3HT:PCBM film with and without differently shaped Ag nanomaterials. As shown in Figure 5a, the absorption intensity of the polymer layer with metallic nanomaterials is stronger than that of pristine P3HT:PCBM. To further clarify our results, we calculate the absorption enhancement by dividing the Ag nanomaterial-doped P3HT:PCBM by that of the pristine P3HT:PCBM. For the Ag nanoparticles-only case, we find one obvious absorption enhancement peak at 620 nm which is different to that of Ag nanoprisms (ca. 400 nm) in water (Figure 2a). Similarly, when Ag nanoprisms are embedded into the active layer, the LSPR shifts to 670 from 600 nm. This red shift can be primarily attributed to the change in refractive index sensed by the Ag nanomaterials due to the change from water to P3HT:PCBM.^[37,39,40]

To understand the details of the absorption enhancement, the theoretical absorption enhancement has been calculated (Figure 5b). A clear absorption enhancement peak around 590 nm is observed for the Ag nanoparticle case, which qualitatively agrees with our experimental results (Figure 5a). For the Ag nanoprism case, the maximum enhancement occurs surrounding 670 and 800 nm, for the transverse magnetic (TM)

Table 1. Photovoltaic parameters of the OSCs with or without Ag nanomaterials incorporated into the active layers under AM 1.5G illumination at 100 mW cm^{-2} . R_s is derived from the slope of the current – voltage (J – V) curves in the dark at 1 V. The OSC devices are control (no Ag nanomaterials), OSCs with weight ratio of 2 wt% Ag nanoparticles only, 2 wt% Ag nanoprisms only, and 2 wt% Ag nanoparticles plus 2 wt% Ag nanoprisms.

Device	V_{oc} [V]	J_{sc} [mA cm^{-2}]	FF [%]	PCE [%]	R_s [$\Omega \text{ cm}^2$]
Without Ag (control)	0.64 ± 0.01	8.99 ± 0.09	62.33 ± 0.57	3.60 ± 0.08	9.89 ± 0.25
Optimized Ag nanoparticle	0.64 ± 0.01	9.80 ± 0.15	63.58 ± 0.54	3.99 ± 0.12	5.58 ± 0.55
Optimized Ag nanoprisms	0.64 ± 0.01	9.93 ± 0.20	64.08 ± 0.66	4.07 ± 0.15	4.54 ± 0.32
Optimized Ag nanoparticle + nanoprisms	0.64 ± 0.01	10.61 ± 0.35	63.33 ± 1.01	4.30 ± 0.20	8.45 ± 0.41

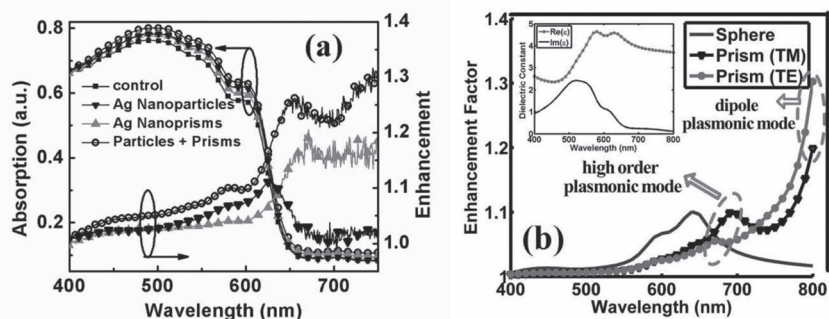


Figure 5. a) UV-vis absorption spectra of P3HT:PCBM film with or without incorporated Ag nanomaterials, and corresponding absorption enhancement. The Ag nanomaterial-doped active layers are 2 wt% Ag nanoparticles only, 2 wt% Ag nanoprisms only, and mixed 2 wt% Ag nanoparticles and 2 wt% Ag nanoprisms. b) The theoretical absorption enhancement of OSCs with nanospheres or nanoprisms embedded into active layer. The inset is the experimentally determined dielectric constant of P3HT:PCBM film.

and transverse electric (TE) modes, respectively. The dipole resonance at 800 nm from nanoprisms cannot overlap the absorption region of active material, making little contribution to absorption enhancement. However, the high-order resonances at 670 nm from prisms contribute to the boosted absorption. The evolutions of dipole and high-order plasmonic resonances from water environment to P3HT:PCBM environment can be comparatively studied in Figure 2b and Figure 5b. Combining the theoretical and experimental studies, we find that: i) the broadband resonance is achieved by the simultaneous excitation of versatile plasmonic resonances, i.e., shape-, size-, and polarization-dependent low- and high-order plasmonic resonances; ii) the low-order mode is dipole resonance, and the high-order mode corresponds to multipole resonance; they show different scattering pattern or angular momentum; and, iii) the low-order mode from nanoprism cannot overlap the absorption region of the active material and makes less contribution to absorption enhancement. Interestingly, the high-order resonances from the nanoprism contribute to the boosted absorption. Consequently, it is reasonable to state that the absorption enhancement coming from the near-field enhancement can be described entirely as a plasmonic effect of the Ag nanomaterials. The light has been concentrated by the plasmon of the Ag nanomaterials, and thus the absorption of medium around the Ag nanomaterials is enhanced, as demonstrated in our experimental and theoretical results.

After studying the optical effect of individual shaped Ag nanomaterials on OSCs, we studied the optical effect of mixed Ag nanomaterials in the active layer (see Figure 5a). It can be observed that a broad absorbance enhancement around wavelength 420–750 nm is clearly obtained. As we know, LPR typically has different resonance wavelength regions depending on metallic material, size, and shape. Our results show that Ag nanoparticles and Ag nanoprisms offer relatively different absorption enhancement regions (Figure 5a). The two shaped Ag nanomaterials complement each other in single junction OSCs to enhance the absorption over a large wavelength region (i.e., achieving a broadband absorption enhancement). To our best knowledge, this is the first time a simple method has been designed to achieve a relatively broadband absorption

enhancement by combining different shaped and sized Ag nanomaterials with different LSPR peak. The broadband resonance is contributed to by the simultaneous excitation of versatile plasmonic resonances, i.e., shape-, size-, and polarization-dependent low- and high-order plasmonic resonances.

Some groups have recently studied plasmonic solar cells by inserting alloy nanoparticles into OSCs, such as Au–Cu alloy nanoparticles, or Au–Ag alloy nanoparticles.^[41,42] Although Au, Cu, and Ag NPs show different LSPR peaks, the alloy cannot be accumulated to produce a broader LPR effect. Very recently, some groups realized a broad scattering effect by designing very large nucleated Ag nanoparticles of 200 nm size in silicon solar cells; unfortunately, the 200 nm sized nanoparticles are too large to be used in nanoscale OSCs.^[20] It is also worth pointing out that the absorption peak of the P3HT is at about 500–550 nm. We adopt mixed Ag nanoparticles (with an absorption of 400 nm) and Ag nanoprisms (with an absorption of 600 nm). Based on the current results, the enhancement peak is at the longer wavelength region around 600 nm because the absorption of material itself at 550 nm is already very high. We would like to enhance the absorption at the wavelength region off the peak of the material absorption.

To further demonstrate the plasmonic effect of the metallic nanomaterials on the optical absorption of OSCs, the monochromatic incident photon-to-electron conversion (IPCE) was investigated, as shown in Figure 6. First, we evaluate the accuracy of J_{sc} of devices by comparing J_{sc} values from J – V characteristics with the calculated J_{sc} from IPCE. The J_{sc} values were calculated by integrating the IPCE data with the AM 1.5G reference spectrum and are rather close to those obtained using J – V measurements (within 4% error). For example, the calculated

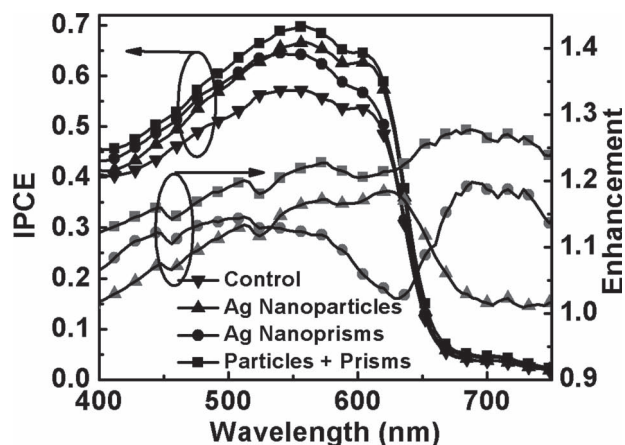


Figure 6. IPCE spectra of OSCs with or without Ag nanomaterials incorporated into the active layer, and corresponding IPCE enhancement. The Ag nanomaterial doped OSCs are 2 wt% Ag nanoparticles only, 2 wt% Ag nanoprisms only, and mixed 2 wt% Ag nanoparticles and 2 wt% Ag nanoprisms.

J_{sc} values of the control, Ag nanoparticles-only, Ag nanoprisms-only, and mixed Ag nanoparticles and Ag nanoprisms devices are 8.65, 9.57, 9.63, and 10.42 mA cm⁻², respectively, which are about 3.93%, 2.41%, 3.11%, and 1.82% lower than the J_{sc} values obtained from the J - V curve. The IPCE results indicate that the photovoltaic results are reliable. Furthermore, from the IPCE results, we find that there is a clear increment when the Ag nanomaterials are incorporated into the active layer for all the cases (Ag nanoparticles only, Ag nanoprisms only, and mixed Ag nanomaterials). The IPCE enhancement of OSCs incorporated with mixed Ag nanomaterials is superior to that of the Ag nanoparticle-only and Ag nanoprism-only OSCs and can cover a broadband wavelength of 400 to 800 nm. By comparing the absorption from Figure 5 with the IPCE spectra of Figure 6, we can see the IPCE enhancement trend is coincident with the absorption enhancement trend while the IPCE enhancement factor is slightly higher than the absorption enhancement factor. The main reason is that IPCE is also partially affected by electrical properties, such as hole and electron transport and collection, apart from the optical properties, as described previously.^[37] Consequently, the observed absorption enhancement via plasmonic effects contribute significantly to the enhancements of J_{sc} , IPCE, and PCE along with the improved electrical properties of increased hole mobilities, electron mobilities, and better balance of electron and hole mobilities, as shown in Figure S4 (see the Supporting Information). It should be noted that the approach of using mixed differently shaped Ag nanomaterials synthesized by a wet solution process is a very simple method for realizing broadband absorption and further improving the device performance. Most importantly, the work contributes to a new route which can inspire researchers to explore the relative project about how to more effectively realize the broadband absorption by realizing simultaneous excitation of versatile plasmonic resonances, i.e., material type, shape, size, environment, and even polarization dependent low- and high-order plasmonic resonances.

3. Conclusions

In this study, a broadband absorption of OSC is realized by combining differently shaped nanomaterials exhibiting varied LPR and scattering region into the active layer. For the Ag nanomaterial-doped OSCs, enhancement of the J_{sc} value for Ag nanoparticles, Ag nanoprisms, and blended Ag NPs is approximately 9.0%, 10.1%, and 17.91%, respectively, compared to the optimized control OSC. As a result, the mixed Ag NPs device shows a high efficiency, with PCE of 4.3%. For the origin of the enhancement, our theoretical and experimental studies show that the broadband resonance is achieved by the simultaneous excitation of versatile plasmonic resonances, i.e., the shape-, size- and polarization-dependent low- and high-order plasmonic resonances. Interestingly, for the Ag nanoprism case, due to the improved overlap with absorption spectrum of the active layer material, the high-order resonances contribute more than low-order resonances to the absorption enhancement of OSCs. Consequently, the results on the mixed plasmonic system confirm that LPR is promising for use in the development of high-performance OSCs. Furthermore, we anticipate that the

scheme of mixing different shaped Ag nanomaterials can contribute to a new route to explore how to better realize the broadband absorption and IPCE in metallic nanomaterial systems. In the future, we could further study cooperative plasmonic effects in metallic nanomaterials with different materials type, shape, size, and even polarization incorporated into active layers or interlayers or both of them.

4. Experimental Section

Synthesis of Ag Nanomaterials: The Ag nanoparticles were synthesized based as previously reported.^[43] In a typical reaction, polyvinylpyrrolidone (PVP) (0.5 g, molecule weight 24 000 g mol; Aladdin, CAS: 9003-39-8) in ethylene glycol (EG, 15 mL) was slowly heated up to ca. 180 °C in a 50 mL vial under vigorous stirring for 20 min (throughout the process, the vial was kept open). Then the temperature was slowly cooled to 120 °C in about 20 min and held at 120 °C. AgNO₃ (0.10 g) in glycol (5 mL) was added drop-by-drop into the solution for about 3 min. The reaction was continued for another 15 min at 120 °C. The generation of brown colloidal dispersion suggested the formation of Ag NPs. After the solution was cooled to room temperature, acetone (40 mL) was added into the Ag nanoparticles solution allowing for the generation of brown precipitate. Then the solution was centrifuged at a speed of 10 000 rpm for 10 min, and the upper solution was removed. After that, ethanol (20 mL) was added into the Ag nanoparticles precipitate and centrifuged at a speed of 10 000 rpm for 10 min. This process was repeated three times. Then, the Ag precipitate was put into a vacuum chamber with a vacuum pressure of 10⁻³ Pa until the Ag nanoparticles become dry. It is important to note that rotary evaporation and thermal treatment should not be used to dry the sample to avoid any possible damage to the Ag nanoparticles. Finally, the Ag nanoparticles were dispersed into a 1, 2-dichlorobenzene (DCB) solution.

Ag nanoprisms were prepared by a photochemical method involving two steps.^[44] First, Ag nanoparticle seeds were prepared as follows: NaBH₄ ice-cold aqueous solution (80 μL, 50 mM) was added to 8 mL silver nitrate solution (0.094 mM) and trisodium citrate (0.28 mM) aqueous solution under vigorous stirring for 10 min. 30 PVP (30 μL, $M_w = 40\,000$ g mol, 0.05 M) aqueous solution was added in. After 30 min stirring, the solution was incubated in a dark environment at 4 °C for 12 h. Then, the bright-yellow solution with small-sized Ag nanoparticle seeds was irradiated by a high brightness LED with 520 nm illumination peak for 10 h after adding NaOH (50 μL, 0.5 M). The solution turned a blueish color, indicating the formation of Ag nanoprisms. The products were purified extensively through repeated washing with water and centrifugation at a speed of 10 000 rpm for 10 min. Then, the Ag precipitate was put into a vacuum chamber with a vacuum pressure of 10⁻³ Pa until the Ag nanoparticles became dry and, finally, the dry Ag nanoprisms were dispersed in DCB solution for device fabrication.

Device Fabrication and Characterization: The original polymer blended solution was prepared by mixing poly(3-hexylthiophene) (P3HT) and phenyl-C61-butyric acid methyl ester (PCBM) at 1:1 ratio, with a total concentration of 50 mg mL⁻¹ (25 mg mL⁻¹ P3HT and 25 mg mL⁻¹ PCBM). To prepare different concentrations of Ag nanomaterials in active layers, 20 μL of Ag nanomaterials in DCB with various NP concentrations were added to 80 μL of P3HT:PCBM in DCB. The final concentration of P3HT and PCBM was 20 mg mL⁻¹. An AFM image of ITO substrate is shown in Figure S5 of the Supporting Information. The root-mean-square (rms) roughness of the ITO is about 1.536 nm. For device fabrication, poly(3,4-ethylenedioxythiophene):poly(styrenesulfonate) (PEDOT:PSS) was first spin-coated onto ITO-coated glass substrate and subsequently annealed at 120 °C for 20 min. Then, the P3HT:PCBM solution with or without Ag NPs was spin-coated onto PEDOT:PSS. After the samples were covered by a small petridish for 1 h, the samples were annealed at 130 °C for 10 min. The resulting thickness of P3HT:PCBM was ca. 220 nm, measured by a Dektak stylus profiler. Incorporation of

Ag NPs does not alter the P3HT:PCBM film thickness. Finally, Ca (80 nm) and Al (100 nm) were sequentially evaporated onto the polymer layer as a cathode to create a device with area 4.5 mm² defined by a shadow mask.

Transmission electron microscopy (TEM) of Ag nanomaterials was performed using a Philips Tecnai G2 20 S-TWIN. The morphology of the active layer was characterized using scanning electron microscopy (SEM; Hitachi S-4800). The absorption spectra of Ag nanomaterials in water were measured on a UV-vis spectrophotometer (UV-1700 Shimadzu). The absorption spectra of the film were extracted from the diffuse reflection (R) and transmission spectra (T) (1-T-R) using a goniometer combined with a CCD spectrometer and integrating sphere. Details of the measurement of J - V characteristics have been described elsewhere.^[7] The IPCE measurement was performed by a system combining xenon lamp, monochromator, chopper, and a lock-in amplifier together with a calibrated silicon photodetector (Hamamatsu mono-Si cell).

Theoretical Modeling: As a rigorous solution to Maxwell's equations, a volume integral equation (VIE) method is developed to characterize the optical absorption of OSCs. Considering non-magnetic optical materials with an arbitrary inhomogeneity profile, the VIE can be written as:

$$E^i(r) = \frac{J}{-i\omega(\varepsilon(\omega) - \varepsilon_0)} - i\omega\mu_0 \int_V \bar{G}(r, r^l) J(r^l) dr^l$$

where $E^i(r)$ is the incident electric field of the light, $\varepsilon(\omega)$ is the position-dependent permittivity of the inhomogeneous materials, J is the volumetric polarization current to be solved, and $\bar{G}(r, r^l)$ is the dyadic Green's tensor in free space. In our model, the polarization currents are expanded using the roof-top vector basis functions;^[45] thus, the continuity of normal current is naturally satisfied at the material interfaces. Furthermore, the hypersingular Green's tensor is smoothed by using the finite-difference approximation. As a traditional iterative solver of the resulting VIE matrix equation, the conjugate-gradient method^[46] converges very slowly and will produce non-physical random errors in the calculation of optical absorption. To tackle the problem, we employ the fast and smoothly converging biconjugate gradient stabilized (BI-CGSTAB) method.^[47] Thanks to the translation-invariant property of free-space Green's function, the fast Fourier transform (FFT) is adopted to accelerate the matrix-vector multiplications encountered in the BI-CGSTAB.^[48]

Supporting Information

Supporting Information is available from the Wiley Online Library or from the author.

Acknowledgements

This work was supported by University Grant Council of the University of Hong Kong (grants #10401466, #201111159062), and the General Research Fund (grants: HKU#712010E and HKU711612E) from the Research Grants Council of Hong Kong Special Administrative Region, PR China. HPH would like to acknowledge a grant "CUHK Group Research Project No. 3110070". WEIS would also like to acknowledge the financial support of National Natural Science Foundation of China (No. 61201122).

Received: August 29, 2012

Revised: October 18, 2012

Published online: January 6, 2013

[1] M. A. Green, S. Pillai, *Nat. Photonics* **2012**, *6*, 130.

[2] X. H. Li, W. C. H. Choy, L. J. Huo, F. X. Xie, W. E. I. Sha, B. F. Ding, X. Guo, Y. F. Li, J. H. Hou, J. B. You, Y. Yang, *Adv. Mater.* **2012**, *24*, 3046.

- [3] D. H. Wang, D. Y. Kim, K. W. Choi, J. H. Seo, S. H. Im, J. H. Park, O. O. Park, A. J. Heeger, *Angew. Chem., Int. Ed.* **2011**, *50*, 5519.
- [4] M. Agrawal, P. Peumans, *Opt. Express* **2008**, *16*, 5385.
- [5] H. A. Atwater, A. Polman, *Nat. Mater.* **2010**, *9*, 205.
- [6] I. Kim, T. S. Lee, D. S. Jeong, W. S. Lee, K. S. Lee, *J. Phys. D: Appl. Phys.* **2012**, *45*, 065101.
- [7] D. D. S. Fung, L. F. Qiao, W. C. H. Choy, C. D. Wang, W. E. I. Sha, F. X. Xie, S. L. He, *J. Mater. Chem.* **2011**, *21*, 16349.
- [8] X. H. Li, W. E. I. Sha, W. C. H. Choy, D. D. S. Fung, F. X. Xie, *J. Phys. Chem. C* **2012**, *116*, 7200.
- [9] F. X. Xie, W. C. H. Choy, C. C. D. Wang, W. E. I. Sha, D. D. S. Fung, *Appl. Phys. Lett.* **2011**, *99*, 153304.
- [10] J. Yang, J. B. You, C. C. Chen, W. C. Hsu, H. R. Tan, X. W. Zhang, Z. R. Hong, Y. Yang, *ACS Nano* **2011**, *5*, 6210.
- [11] J. You, X. Li, F. X. Xie, W. E. I. Sha, J. H. W. Kwong, G. Li, W. C. H. Choy, Y. Yang, *Adv. Energy Mater.* **2012**, *2*, 1203.
- [12] D. H. Wang, J. K. Kim, G.-H. Lim, K. H. Park, O. O. Park, B. Lim, J. H. Park, *RSC Adv.* **2012**, *2*, 7268.
- [13] C. H. Kim, S. H. Cha, S. C. Kim, M. Song, J. Lee, W. S. Shin, S. J. Moon, J. H. Bahng, N. A. Kotov, S. H. Jin, *ACS Nano* **2011**, *5*, 3319.
- [14] A. J. Morfa, K. L. Rowlen, T. H. Reilly, M. J. Romero, J. van de Lagemaat, *Appl. Phys. Lett.* **2008**, *92*, 013504.
- [15] J. N. Pei, J. L. Tao, Y. H. Zhou, Q. F. Dong, Z. Y. Liu, Z. F. Li, F. P. Chen, J. B. Zhang, W. Q. Xu, W. J. Tian, *Sol. Energy Mater. Sol. Cells* **2011**, *95*, 3281.
- [16] W. E. I. Sha, W. C. H. Choy, Y. P. P. Chen, W. C. Chew, *Opt. Express* **2011**, *19*, 15908.
- [17] Z. Ye, S. Chaudhary, P. Kuang, K. M. Ho, *Opt. Express* **2012**, *20*, 12213.
- [18] L. Muller-Meskamp, Y. H. Kim, T. Roch, S. Hofmann, R. Scholz, S. Eckardt, K. Leo, A. F. Lasagni, *Adv. Mater.* **2012**, *24*, 906.
- [19] J. L. Wu, F. C. Chen, Y. S. Hsiao, F. C. Chien, P. L. Chen, C. H. Kuo, M. H. Huang, C. S. Hsu, *ACS Nano* **2011**, *5*, 959.
- [20] X. Chen, B. H. Jia, J. K. Saha, B. Y. Cai, N. Stokes, Q. Qiao, Y. Q. Wang, Z. R. Shi, M. Gu, *Nano Lett.* **2012**, *12*, 2187.
- [21] S. S. Kim, S. I. Na, J. Jo, D. Y. Kim, Y. C. Nah, *Appl. Phys. Lett.* **2008**, *93*, 073307.
- [22] B. V. K. Naidu, J. S. Park, S. C. Kim, S. M. Park, E. J. Lee, K. J. Yoon, S. J. Lee, J. W. Lee, Y. S. Gal, S. H. Jin, *Sol. Energy Mater. Sol. Cells* **2008**, *92*, 397.
- [23] D. H. Wang, K. H. Park, J. H. Seo, J. Seifert, J. H. Jeon, J. K. Kim, J. H. Park, O. O. Park, A. J. Heeger, *Adv. Energy Mater.* **2011**, *1*, 766.
- [24] X. H. Li, G. Y. Chen, L. B. Yang, Z. Jin, J. H. Liu, *Adv. Funct. Mater.* **2010**, *20*, 2815.
- [25] S. S. Kim, S. I. Na, J. Jo, D. Y. Kim, Y. C. Nah, *Appl. Phys. Lett.* **2008**, *93*, 073307.
- [26] B. Wu, T. Z. Oo, X. L. Li, X. F. Liu, X. Y. Wu, E. K. L. Yeow, H. J. Fan, N. Mathews, T. C. Sum, *J. Phys. Chem. C* **2012**, *116*, 14820.
- [27] R. S. Kim, J. F. Zhu, J. H. Park, L. Li, Z. B. Yu, H. J. Shen, M. Xue, K. L. Wang, G. Park, T. J. Anderson, Q. B. Pei, *Opt. Express* **2012**, *20*, 12649.
- [28] S. Shahin, P. Gangopadhyay, R. A. Norwood, *Appl. Phys. Lett.* **2012**, *101*, 053109.
- [29] T. Z. Oo, N. Mathews, G. C. Xing, B. Wu, B. G. Xing, L. H. Wong, T. C. Sum, S. G. Mhaisalkar, *J. Phys. Chem. C* **2012**, *116*, 6453.
- [30] J. Zhu, M. Xue, R. Hoekstra, F. Xiu, B. Zeng, K. L. Wang, *Nanoscale* **2012**, *4*, 1978.
- [31] G.-Q. Fan, Q.-Q. Zhuo, J.-J. Zhu, Z.-Q. Xu, P.-P. Cheng, Y.-Q. Li, X.-H. Sun, S.-T. Lee, J.-X. Tang, *J. Mater. Chem.* **2012**, *22*, 15614.
- [32] X. Yang, A. Uddin, M. Wright, *Phys. Status Solidi – R* **2012**, *6*, 199.
- [33] G. D. Spyropoulos, M. M. Stylianakis, E. Stratakis, E. Kymakis, *Appl. Phys. Lett.* **2012**, *100*, 213904.
- [34] J. A. Schuller, E. S. Barnard, W. S. Cai, Y. C. Jun, J. S. White, M. L. Brongersma, *Nat. Mater.* **2010**, *9*, 193.

- [35] W. Wang, S. M. Wu, K. Reinhardt, Y. L. Lu, S. C. Chen, *Nano Lett.* **2010**, *10*, 2012.
- [36] Z. Ye, S. Chaudhary, P. Kuang, K. M. Ho, *Opt. Express* **2012**, *20*, 12213.
- [37] C. C. D. Wang, W. C. H. Choy, C. Duan, D. D. S. Fung, W. E. I. Sha, F.-X. Xie, F. Huang, Y. Cao, *J. Mater. Chem.* **2012**, *22*, 1206.
- [38] V. D. Mihailetchi, J. Wildeman, P. W. M. Blom, *Phys. Rev. Lett.* **2005**, *94*, 126602.
- [39] A. P. Kulkarni, K. M. Noone, K. Munechika, S. R. Guyer, D. S. Ginger, *Nano Lett.* **2010**, *10*, 1501.
- [40] M. Stavitska-Barba, M. Salvador, A. Kulkarni, D. S. Ginger, A. M. Kelley, *J. Phys. Chem. C* **2011**, *115*, 20788.
- [41] H. C. Chen, S. W. Chou, W. H. Tseng, I. W. P. Chen, C. C. Liu, C. Liu, C. L. Liu, C. H. Chen, C. I. Wu, P. T. Chou, *Adv. Funct. Mater.* **2012**, *22*, 3975.
- [42] M. Heo, H. Cho, J. W. Jung, J. R. Jeong, S. Park, J. Y. Kim, *Adv. Mater.* **2011**, *23*, 5689.
- [43] L. Li, J. Sun, X. R. Li, Y. Zhang, Z. X. Wang, C. R. Wang, J. W. Dai, Q. B. Wang, *Biomaterials* **2012**, *33*, 1714.
- [44] C. Xue, C. A. Mirkin, *Angew. Chem., Int. Ed.* **2007**, *46*, 2036.
- [45] A. W. Glisson, D. R. Wilton, *IEEE Trans. Antennas Propag.* **1980**, *28*, 593.
- [46] M. R. Hestenes, E. Stiefel, *J. Res. Nat. Bur. Stand.* **1952**, *49*, 409.
- [47] H. A. Vandervorst, *SIAM J. Sci. Stat. Comput.* **1992**, *13*, 631.
- [48] M. F. Catedra, E. Gago, L. Nuno, *IEEE Trans. Antennas Propag.* **1989**, *37*, 528.